Study on Current Collector and Electrolyte Design/Electrochemical Behaviour of an In-Plane Lignin derived Laser Scribed Graphene for Microsupercapacitor Application

Sathaniswarman Remesh[a,b,#], Mugashini Vasudevan[a,b,#], Veeradasan Perumal[a,b,*], Thomas Nesakumar Jebakumar Immanuel Edison[c], Pandian Bothi Raja[d], Mohamad Nasir Mohamad Ibrahim[d], Saravanan Karuppanan[a,b], Mark Ovinis[e], Natarajan Arumugam[f], Raju Suresh Kumar[f]

[a] Centre of Innovative Nanostructures and Nanodevices (COINN), Universiti Teknologi PETRONAS, 32610 Seri Iskandar, Perak Darul Ridzuan, Malaysia

[b] Department of Mechanical Engineering, Universiti Teknologi PETRONAS, 32610 Seri Iskandar, Perak Darul Ridzuan, Malaysia

[c] Department of Chemistry, Sethu Institute of Technology, Kariapatti 626115, Virudhunagar District, Tamil Nadu, India

[d] School of Chemical Sciences, Universiti Sains Malaysia, 11800 Penang, Malaysia

[e] School of Engineering and the Built Environment, Faculty of Computing, Engineering and the Built Environment, Birmingham City University, B4 7XG, UK

[f] Department of Chemistry, College of Science, King Saud University, P.O. Box 2455, Riyadh 11451, Saudi Arabia

#These authors contribute equally to this work.

*Corresponding author at: Centre of Innovative Nanostructures and Nanodevices (COINN), Universiti Teknologi PETRONAS, 32610 Seri Iskandar, Perak Darul Ridzuan, Malaysia

Email address: veeradasan.perumal@utp.edu.my

Abstract

Current collectors and electrolyte pairs are frequently overlooked in the development of supercapacitors. For electrode design and sealed packaging, the mechanical and chemical properties of the electrolyte must be retained while maintaining the integrity of microelectrodes and current collectors of the microsupercapacitors. In this research, the physical and electrochemical response of copper (Cu) and 316 stainless steel current collector (SS) was studied, for lignin-derived laser scribed graphene (L-LSG) microsupercapacitor with K_2SO_4 (K^+) and H_2SO_4 (H^+) as an electrolyte medium. XPS results confirmed a passivation layer on a copper electrode both before and after the electrochemical reaction involving H_2SO_4 as the electrolyte medium of the highly porous L-LSG structure with six pairs of microelectrodes and graphene current collectors. Analysis of the CV and GCD curves shows that the SS/K^+ pair is the most suited for an L-LSG microsupercapacitor, with an areal capacitance of 22.22 $mFcm^{-2}$ at 0.08 $mAcm^{-2}$.

Keywords — Laser Scribed Graphene; Lignin; Stainless Steel; Microsupercapacitor.

1.0 Introduction

Almost all consumer applications in this twenty-first century require effective energy charging, discharging, and storage components. For instance, a mobile phone includes a rechargeable battery that allows it to charge and utilize the stored energy for a set amount of time. Recent studies have found that batteries struggle to keep up with the energy generated by renewable energy sources such as wind turbines and hydroelectric generators because their intensity and direction fluctuate over time [1]. Although these processes have been accomplished on a low-power scale using batteries, new ways for increasing efficiency will require enormous quantities of power that can only be delivered by alternative energy storage technologies such as supercapacitors [1].

Supercapacitors have been described as the electrical component of the future that bridges the gap between batteries and capacitors due to their high energy and power density and long cycling stability [2]. Supercapacitors can be divided into two main categories: pseudocapacitors and electrochemical double-layer capacitors (EDLC). While a pseudocapacitor mainly utilizes a redox mechanism through metal and polymers, EDLC relies on ion exchange of porous carbon materials with larger surface areas [3]. Despite the high-power density and extended life cycle of supercapacitors, they are limited by their low energy density [1]. Thus, to further increase the energy and power density, and cycle stability of supercapacitors, multiple studies have been undertaken combining EDLC with pseudocapacitive materials to create hybrid supercapacitors. A hybrid supercapacitor incorporates properties from both supercapacitor types, making it on par or even superior to batteries in terms of longevity, power output and rechargeability.

Geim and Novaselov's remarkable discovery of mechanical exfoliation to produce graphene has revolutionized the use of graphene as an EDLC material for supercapacitor applications [4]. The exceptional characteristics of graphene, a single sheet of carbon atoms structured in a honeycomb lattice, make it valuable for various applications [5]. Laser lithography technology stands out as the most feasible graphene synthesis technique, as it is reasonably priced, and, most significantly, capable of generating continuous patterns of microelectrodes through addition, subtraction, and modification, creating several types of hybrid supercapacitors [6,7]. Recently, laser scribing of functionalized graphene from a mixture of flexible polymer and lignin as a carbon substrate has been achieved, with strong bonding established to anchor hybrid materials on top of the induced defects found on functionalized graphene, allowing for biowaste recycling and green electronics [8,9]. Moreover, the large surface area of the extremely porous graphene (meso and micro) created by the laser scribing method enhances ion exchange during the charge and discharge process [7,10].

However, the use of microsupercapacitors is severely hampered by electrolyte leakage and current collector corrosion in polyimide packaging [11]. A key element in maintaining the electrochemical performance involves suitable electrolyte selection. Additionally, the current collector should be considered as well, since damage from corrosion caused by electrolytes may alter the fabricated material and affect the system's overall performance [12]. For instance, metal corrosion by water-based or highly acidic electrolytes could dissolve impurities in the medium, which can alter the morphology of the hybrid device and influence the overall resistance [12,13]. The damage done to the current collector is irreversible and could reduce the microsupercapacitor lifespan.

This study showcases the utilization of an affordable current collector that is highly resistant to corrosion (Stainless Steels), as well as a unique neutral electrolyte (PAAS/K_2SO_4), for the application of microsupercapacitors composed of laser-scribed graphene derived from oil palm lignin. This work serves as the foundation for our newly reported optimized oil palm lignin derived laser scribed graphene employing neutral electrolyte [14]. The selection of the current collector and electrolyte combination is a critical yet frequently overlooked aspect, which may lead to deterioration and self-discharge issues. The application of H_2SO_4 on a lignin electrode has been reported to cause protonation of the lignin functions and cleavage of the bonds present in lignin, hence hindering lignin's ability to operate at its highest capacity [15,16]. We take into account the selection of a suitable mix of electrolyte and current collector for the frequently used lignin-derived laser scribed graphene in literature. The study used six paired microelectrode supercapacitors using copper (Cu) or stainless steel (SS) as the current collector and PVA/H_2SO_4 (H^+) or PAAS/ K_2SO_4 (K^+) as the electrolyte pair. The SS/K^+ pair has demonstrated an exceptional areal capacitance of 22.22 $mFcm^{-2}$ at a current density of 0.08 $mAcm^{-2}$. The utilization of PAAS/K_2SO_4 as a gel electrolyte and SS as a current collector, in conjunction with biopolymer-derived graphene, is least reported in any literature study.

2.0 Methods and Experiments

2.1 Materials and chemicals

Lignin was extracted from empty fruit bunches of oil palm [17]. Materials such as copper tape (Cu), 316 stainless steels (SS) were obtained from a local supplier. Chemicals such as Potassium Sulphate (K_2SO_4), Sulphuric acid (H_2SO_4), Polyvinyl alcohol (PVA) and Sodium polyacrylate (PAAS) were purchased from Sigma-Aldrich. Distilled water and 95% ethanol were used throughout the experiment for sterilization and dilution. All these chemicals were used as received without additional purification.

2.2 Preparation of electrode drawing for laser writing

CorelDRAW X6 software was utilized to construct an interdigitated electrode consisting of six pairs of electrodes. The electrode is 9.4 mm wide overall and has a maximum height of 6.8 mm. The width and thickness of each microelectrode were kept constant at 3.0 mm and 0.25 mm. The micro gap between the electrodes is maintained at 0.3 mm. A thicker current collector with a measurement of 3.0 mm is used to ensure maximum contact with conducting wires/tapes.

2.3 Fabrication of lignin derived graphene

Lignin powder was diluted in distilled water at a concentration of 20 % (v/v). Meanwhile, an ITO glass was overlaid with a flexible polyimide substrate for drop coating. Before starting the laser scribing, lignin solution was applied to the substrate and dried at 50 °C until the coating was completely dry. The substrate was laser scribed at the appropriate laser intensity (18 W) and speed (40%) using a CO2 laser (V-460, Universal Laser System, 30 W). The final product was cleaned using a water bath to eliminate untreated impurities and was labelled as L-LSG.

2.4 Development of microsupercapacitor packaging

After being laser scribed, the microelectrodes were packed using two distinct current collectors, namely copper tape and 316 stainless steels. Silver paste and polyimide tape were used to adhere the metal conductors to the current collector, and they were allowed to dry for a few hours before applying the electrolyte. Two gel-like electrolytes, PVA/H_2SO_4 and PAAS/K_2SO_4, were developed for this experiment. The 1 M PVA/H_2SO_4 electrolyte was created by mixing 1 g of PVA with 10 ml of water and 1 ml of H_2SO_4 at 1000 rpm at 85 °C for 4 hours. Meanwhile, 0.5 M K_2SO_4 solution was mixed with Sodium polyacrylate at room temperature to obtain PAAS/K_2SO_4 electrolyte.

2.5 Characterization

Field Emission Scanning Electron Microscopy (VP-FESEM) (TESCAN CLARA, UHR SEM) was used to analyze the surface morphology of the material. X-ray Photoelectron Spectroscopy (XPS) by Thermo Scientific K-Alpha was used to obtain the chemical composition of the material. All Cyclic Voltammetry (CV) and Galvanostatic Charge-Discharge (GCD) (Metrohm Multi Autolab M204 Potentiostat/Galvanostat) were carried out at a voltage window - 0.4 V to 0.4 V to determine the electrical performance of the developed microsupercapacitors. The GCD curves were performed at a current density of 0.08 to 1.0 $mAcm^{-2}$, while the CV curves were assessed at a scan rate of 10 to 200 mVs^{-1}. All the physical and electrochemical characterizations were carried out at room temperature.

3.0 Result and Discussion

This work demonstrates the use of a novel neutral electrolyte and a low-cost, highly corrosion-resistant current collector for microsupercapacitors constructed from laser-scribed graphene derived from oil palm lignin. Figure 1 depicts the fabrication and packaging of L-LSG into the microsupercapacitor. An oil palm lignin solution is initially applied to the polyimide sheet and allowed to dry. Functionalized microelectrodes composed specifically of hydroquinone/quinone group for redox activity were laser scribed on the thin film. Graphene microelectrodes linked to two different current collector materials (copper and stainless steel), and two electrolytes (PVA/H_2SO_4 and PAAS/K_2SO_4) will be applied to each. Following a 4-hour soak up at room temperature, the synthesized microsupercapacitors packed with gel electrolytes were electrochemically characterized. The procedure and other key elements are described in the method and experiment section.

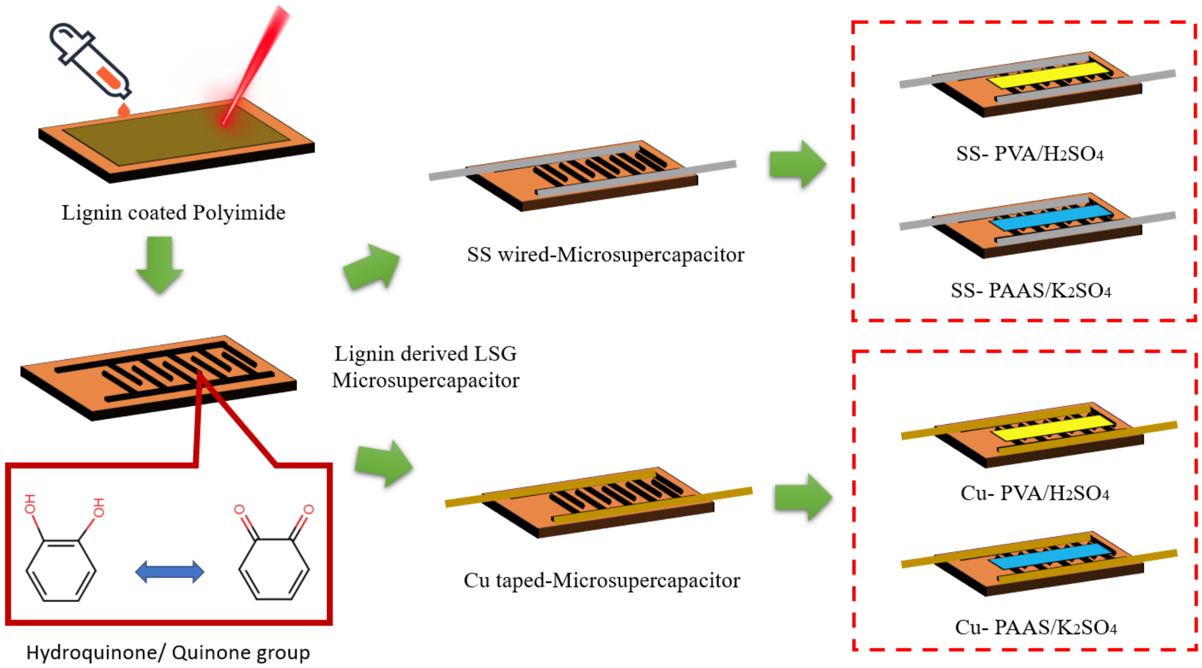

Fig.1 Schematic illustration of the fabrication and packaging of L-LSG microsupercapacitor

3.1 Field Emission Scanning Electron Microscopy (FESEM)

Figure 2 shows the FESEM image of the L-LSG electrode constructed using the laser scribing technique. The microelectrode pattern is shown in Fig. 2a with no overlapping connections between the anode and cathode to prevent a short circuit. Fig. 2b shows the laser writing tool's micrometer accuracy and the consistency of electrode thickness (312 µm) and gap measurements (241 µm). As a result of continuous laser scribing from left to right, a wave-like pattern with a 3D hierarchical structure is created (Fig. 2c). The magnified image of L-LSG in Fig. 2d shows multiple macros and mesopores, due to the instant evaporation of gas molecules during laser writing process [6]. The blend of graphene's porous and fibrous structures assisted in the diffusion of ions during electrochemical processes [8]. Wide gaps between the nearby fiber offer an excellent basis for the development of composite materials, which further boost the energy storage properties of graphene.

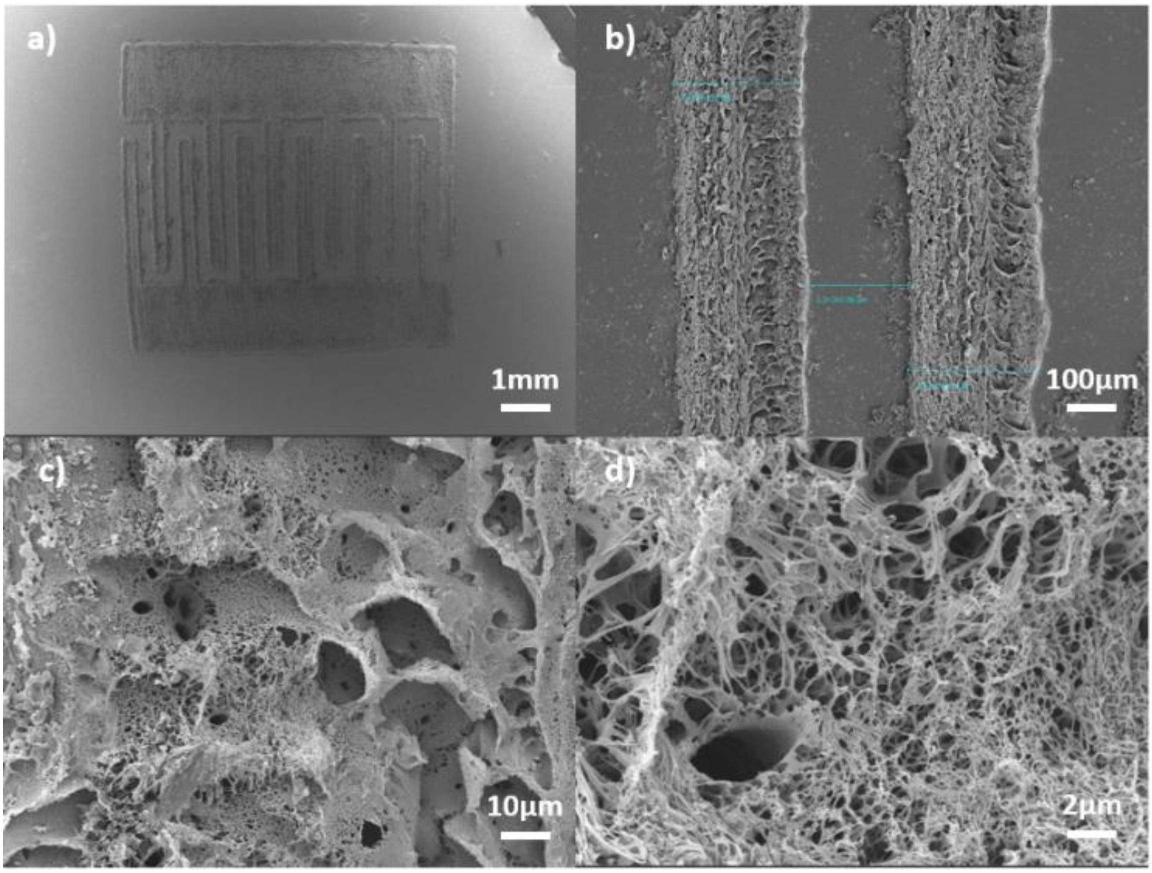

Fig.2 FESEM images of L-LSG electrode. (a) Top view. (b) Gap and microelectrode thickness measurement. (c,d) Magnified images corresponding to the microelectrode.

3.2 Energy Dispersive X-ray Spectrometry (EDS) and Elemental Mapping

The L-LSG Energy Dispersive X-ray Spectrum in Fig. 3a shows 4 distinct peaks of C, O, Na, and Au. Since it is assumed to be a byproduct of sample processing, the non-labelled gold particle (Au) peak at around 2.2 keV has been disregarded [18]. It is apparent that the resultant L-LSG is rich in carbon, and the presence of oxygen suggests the existence of functional groups originating from oil palm lignin. The presence of contaminants from the lignin extraction by soda pulping procedure resulted in the detection of Na and S peak with a rather low intensity [19,20]. The elemental mapping depicted in Fig. 3b-e revealed that the carbon and oxygen functionality groups were spread equally across the L-LSG.

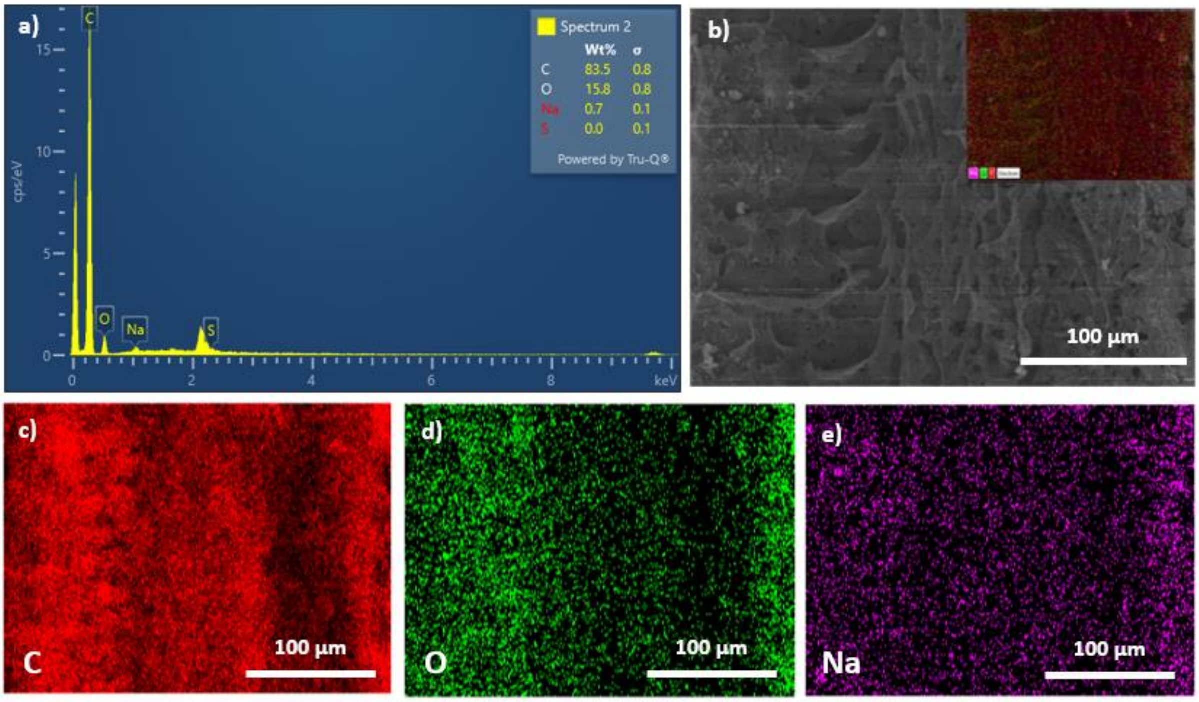

Fig. 3. (a) EDS and (b-e) Elemental Mapping of L-LSG.

3.3 Raman Spectroscopy

In the Figure 4, the first peak D, (~1352 cm^{-1}) formed to due defects and bent of sp^2 bonds found on the produced L-LSG [10]. The defects might have occurred due to irregular laser power and speed during the laser scribing process. Moreover, different lignin oxygen functionalities may be present inside the graphene sheet, occupying the vacancies of the sp^2 bonded carbon, which might be another defect for the creation of the D peak [21]. The second peak G forms at a Raman shift of ~1579 cm^{-1} and confirms the presence of first order sp^2 hybridized carbon [9,10]. In addition, the peak is also related to the ordered graphite in-plane vibrations with E2g symmetry (phonons of sp^2 atoms) [22]. The intensity of the G peak will also increase when high-quality graphene is produced at the optimum laser power and speed. The third peak 2D (~2690 cm^{-1}) is responsible for the formation of multiple layers of graphene to form graphite [23]. The effective thickness of the graphene layer formed was calculated by the ratio (I_G/I_{2D}). The lower the value of (I_G/I_{2D}), the lower the number of graphene layers were formed [22]. The calculated value of (I_G/I_{2D}) is 2.31. In addition, the lower ratio of (I_D/I_G) can be used to evaluate high-quality graphene where it can be used to calculate crystalline structure, La [22]. The calculated value of (I_D/I_G) is 0.86. On other hand, La has been calculated and it has a value of 22.34 nm

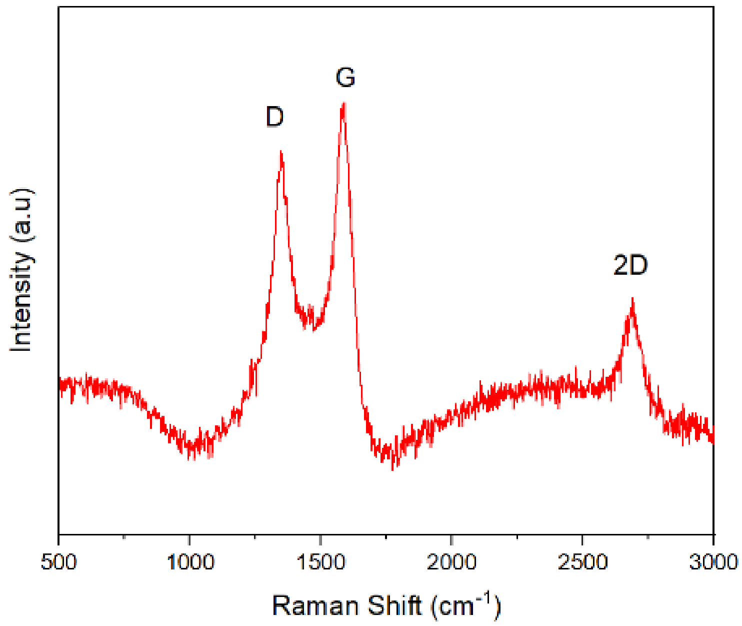

Fig.4. Raman Spectrum of L-LSG

3.4 X-ray Photoelectron Spectroscopy (XPS)

Fig. 5a depicts a fabricated L-LSG microsupercapacitor constructed of two different types of current collector, the 316 SS wire and copper tape. The complete polyimide encapsulation has prevented electrolyte leakage and short circuit. Two primary peaks identified as C and O at 285.08 eV and 532.11 eV, respectively, are apparent in the XPS survey spectra on the outer layer of 316 SS wire [24] (Fig. 5b). The metal surface of stainless steel is hardly exposed, making it resistant to corrosive substances. On the other hand, the copper tape's 935.14 eV XPS survey peak is indicative of copper exposure on top of carbon and oxygen before and after electrochemical performance [25] (Fig. 5c and d). The passive layer on top of copper tape has been identified as CuO (before) and Cu_2O (after), which resulted from redox reactions with atmospheric moisture and sulfuric acid, respectively. Fig. 5e and f show a comparison of Cu 2p and O 1s spectra of both samples. The CuO possesses 4 distinguishable peaks of Cu 2p $_{3/2}$ (933.72 eV), Cu 2p $_{1/2}$ (953.5 eV) and Cu^{2+} satellite peaks (942.58 and 962.6 eV), while Cu_2O possesses only 2 clear peaks of Cu 2p $_{3/2}$ (932.6 eV) and Cu 2p $_{1/2}$ (952.4 eV) [26–28]. The sample primarily included Cu (I) oxidation, as demonstrated by the lack of $Cu2^{+}$ satellite peaks for Cu_2O [29]. The slight variation in the peak of O 1s from 531.48 eV to 532.15 eV further proves the shift in oxidation states of copper ion [27,28].

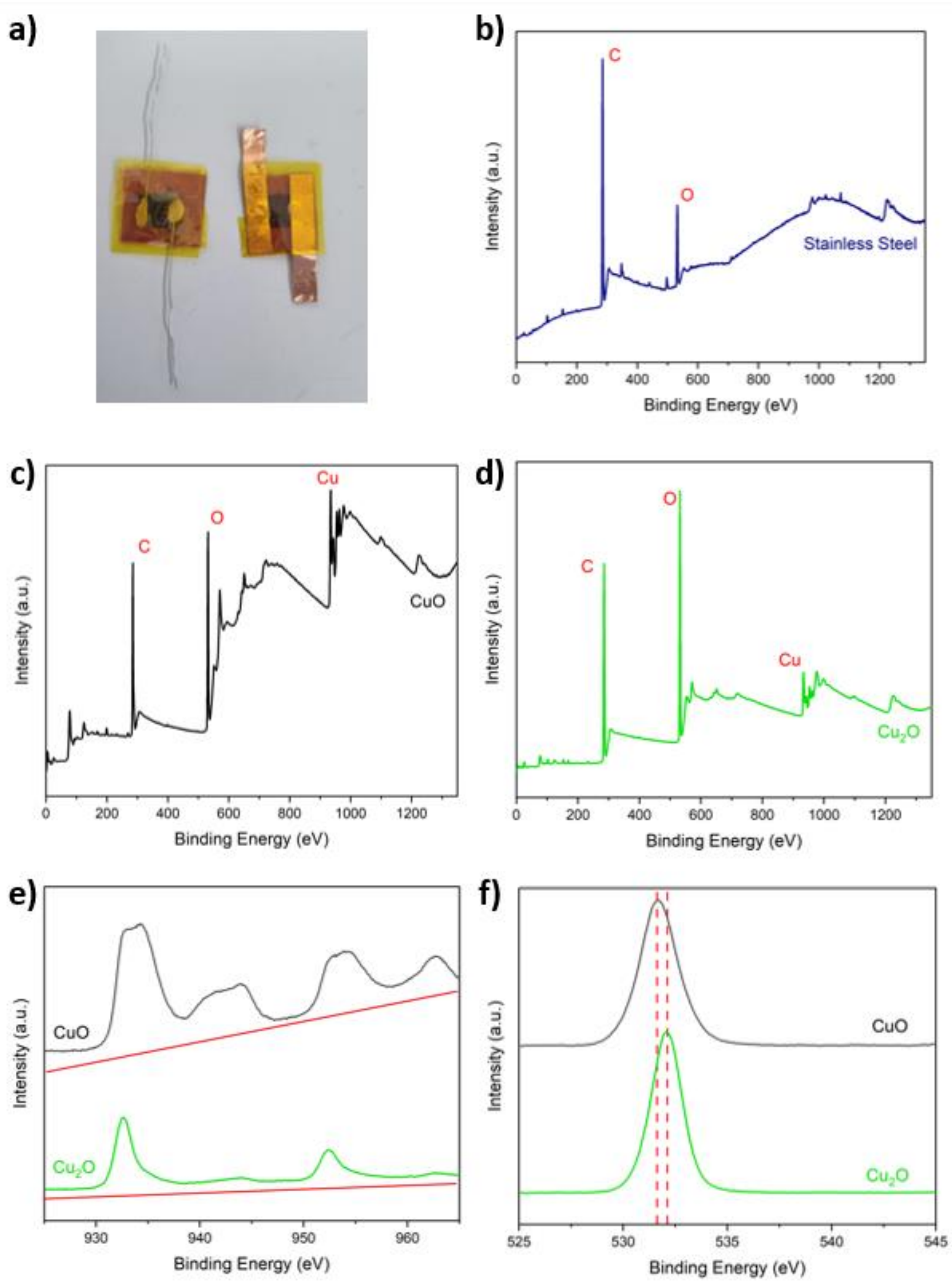

Fig. 5. (a) L-LSG microsupercapacitor comprised of 316 SS wire (left) and copper tape (right). XPS survey spectra of 316 SS (b), Cu tape before electrochemical studies (c) and Cu tape after electrochemical studies (d). Cu 2p (e) and O 1s (f) spectra of Cu tape before and after electrochemical studies.

3.4 Cyclic Voltammetry (CV)

The cyclic voltammetry diagram of various current collectors and electrolytes measured at 50 mVs^{-1} is shown in Fig. 6a and b. Cu/H^+ has the largest CV area of any of the other couples, primarily due to its significant redox activity with H_2SO_4, resulting in the formation of Cu2O based on the equation (1) below [30].

$$\text{Equation: } Cu\ (s) + H_2SO_4\ (l) \rightarrow Cu_2O\ (s) + SO_2\ (g) + H_2O \qquad (1)$$

SS/K^+ and Cu/K^+ exhibit redox peaks due to the presence of aromatic lignin-derived compounds called hydroquinone [31,32]. Furthermore, no redox peaks were identified in the SS/ H^+ peaks due to the development of cleavage and protonation between aromatic compounds prevalent in lignin, lowering its redox reactivity [15,16]. At a potential window of 0.8 V, combining the neutral electrolyte K_2SO_4 with the non-corrosive metal stainless steel yielded highly stable CV curves with balanced OER and HER activity [33]. Cu/H^+, SS/K^+ possess the highest areal capacitance of 2.75 $mFcm^{-2}$ followed by Cu/K^+ (2.19 $mFcm^{-2}$) and SS/H^+ (1.97 $mFcm^{-2}$), respectively. The further analysis of SS/K^+ at various scan rates is shown in Fig. 6c. Fig. 6d indicates that among all the current collectors and electrolytes tested, the SS and K^+ electrolyte's synergistic effect delivered the most stable areal capacitance throughout scan rates of 0 to 200 mVs^{-1}.

3.5 Galvanostatic Charge Discharge (GCD)

Fig. 6e illustrates the GCD curves for the various current collectors and electrolytes recorded at 0.1 $mAcm^{-2}$. Due to the pseudocapacitive qualities of the lignin compound obtained during the laser scribing process, SS/K^+ and Cu/K^+ exhibit an irregular triangle shaped GCD [31,32]. As per CV results, corrosion in the case of Cu/H^+ led to significantly increased reactivity in GCD curves. SS/H^+ or Cu/K^+ is a promising electrode since an acidic or water-based environment could cause SS and Cu to corrode and form a passivation layer [12,13]. SS/K^+ exhibits the second greatest areal capacitance of 21.28 $mFcm^{-2}$ at 0.1 $mAcm^{-2}$ due to the absence of a passivation layer, consistent with past CV findings. Moreover, the GCD of SS/K^+

performed well at varied current densities and showed a substantially greater areal capacitance of 22.22 $mFcm^{-2}$ at 0.08 $mAcm^{-2}$ (Fig. 6f). The energy and power density of the fabricated microsupercapacitor reaches a maximum of 0.00153 $mWhcm^{-2}$ at a power density of 0.25 $mWcm^{-2}$. The areal capacitance of fabricated microsupercapacitor was compared with existing laser scribed graphene-based supercapacitors or similar microsupercapacitors found in literature (Table 1). The L-LSG SS/K+ microsupercapacitor exhibited similar performance to the Co_3O_4/LIG -80 [34], Ph-ddm/LIG [35], and LSG-P24-Au [8] equivalents, without the need for copper current collector or other commonly employed acidic electrolytes. The areal capacitance of laser scribed graphene derived from oil palm lignin has been enhanced by roughly 40% by further optimization [14].

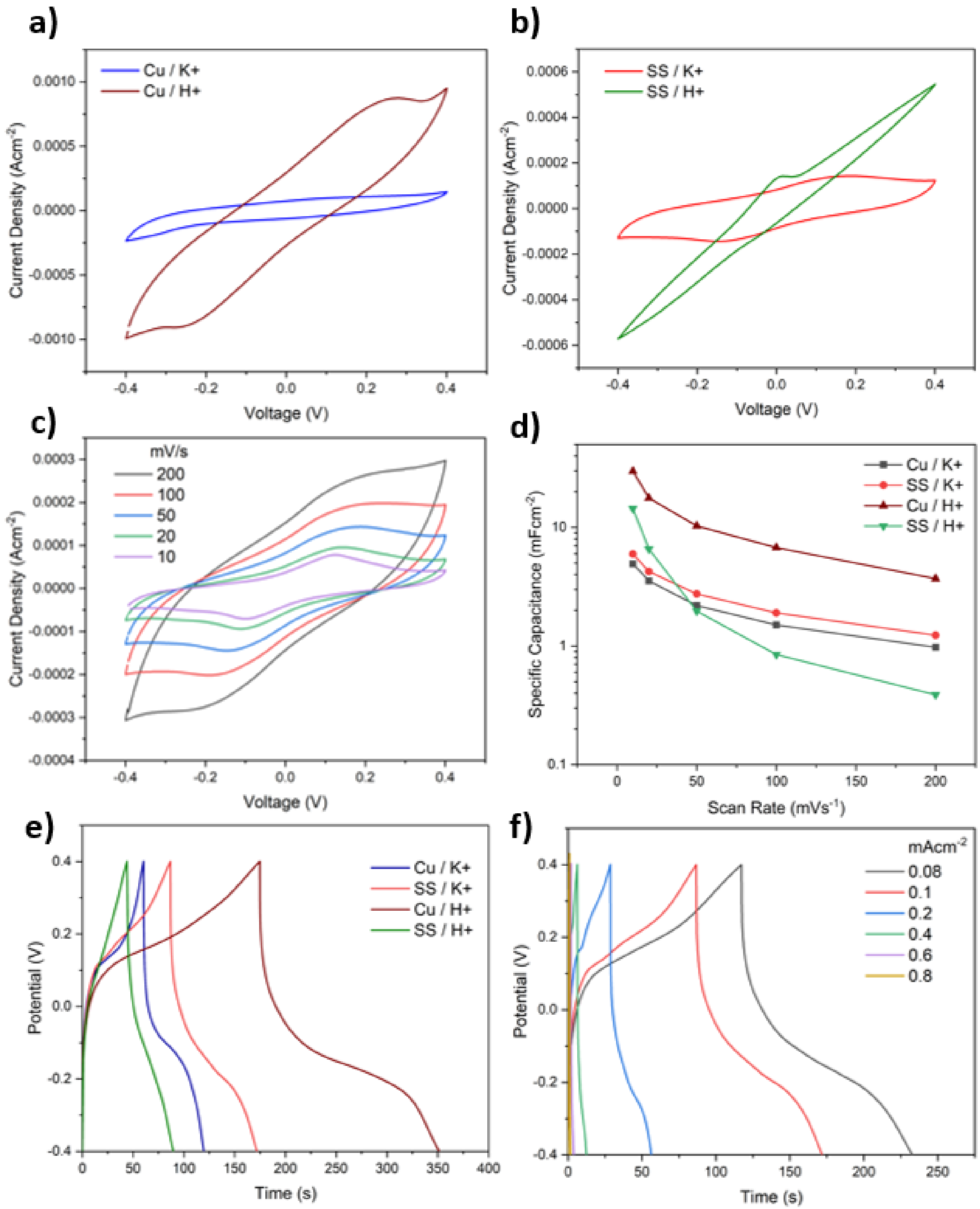

Fig. 6. Cyclic Voltammetry of L-LSG from Cu (a) and SS (b) current collector under different electrolytes at 50 mVs^{-1}. Cyclic Voltammetry of SS/K^{+} at multiple scan rates (c). Areal capacitance of fabricated samples at multiple scan rates (d). Galvanostatic Charge Discharge curves of L-LSG comprising Cu/K^{+}, SS/K^{+}, Cu/H^{+} and SS/H^{+} at 0.1 mAcm^{-2} (e). Galvanostatic Charge Discharge of SS/K^{+} at multiple current densities (f)

292 *Table 1 Comparison of the electrochemical performance of L-LSG (SS/K^+) with other reported*
293 *laser scribed graphene microsupercapacitor.*

Type of electrode	Current Density ($mAcm^{-2}$)	Areal Capacitance ($mFcm^{-2}$)	Highest Energy Density ($mWhcm^{-2}$)	Current Collector	Electrolyte	Ref
L-LSG (SS/K^+)	0.08	22.22	0.00153	SS	K_2SO_4/PAAS	This work
OPL-LSG 7030	0.08	30.77	0.00176	SS	K_2SO_4/PAAS	Previous Work [14]
Co_3O_4/LIG -80	0.05	22.3	-	Cu	H_3PO_4/PVA	[34]
Ph-ddm/LIG	0.2	22.2	~0.004	Cu	BMIM-BF4	[35]
M-PBV-RGO	0.1	17.9	0.00249	Cu	H_2SO_4/PVA	[36]
5B-LIG	0.05	16.5	~0.002	Cu	H_2SO_4/PVA	[37]
KOH-LIG	0.05	32	0.00427	Cu	H_3PO_4/PVA	[38]
PA-PBI-LIG	0.05	14.55	0.00196	Cu	H_2SO_4	[39]
SN-LrGO	0.125	11.35	-	Cu	H_3PO_4/PVA	[40]
LSG-P24-Au	0.02	25.1	0.0036	Cu	H_2SO_4/PVA	[8]
LSG-P24	0.05	17.0	0.0026	Cu	H_2SO_4/PVA	[8]
LIG	0.2	3.9	~0.0004	Cu	H_2SO_4	[10]

Conclusion

In conclusion, due to the neutral and non-corrosive qualities, stainless steel and K_2SO_4 is an effective electrode/electrolyte combination. Microelectrode and current collector material degradation has been avoided using environmentally friendly K_2SO_4, rather than an alternate acid or base electrolyte. Using stainless steel as the primary electrode material has improved the supercapacitor, since it inhibits corrosion induced by the electrolyte leaking through porous graphene. The lifespan of the microsupercapacitor can be prolonged further by optimizing the current collector and electrolyte and reducing self-discharge over time. According to FESEM data, laser scribing the biowaste generated a perfect microelectrode with ample space to attach current collectors. The XPS findings have provided us with further details on how the electrochemical process generates passive layers, affecting the overall charge and discharge parameters of L-LSG, as evidenced in CV and GCD measurements. Future studies need to enhance the microsupercapacitor's encapsulation to prevent electrolyte leakage and external contamination.

Acknowledgement

The authors would like to express their gratitude to Universiti Teknologi PETRONAS (UTP) and Yayasan Universiti Teknologi PETRONAS (YUTP) for financing the research under grant number YUTP-FRG 015CL0-454. The authors gratefully thank funding from King Saud University's Researchers Supporting Project Number (RSP2023R143), Riyadh, Saudi Arabia. The whole team and staff at the UTP's Department of Mechanical Engineering and Centre of Innovative Nanostructures & Nanodevices (COINN) should also be thanked.

Conflict Of Interest

The authors hereby declare that there is no conflict of interest.

References

[1] González A, Goikolea E, Barrena JA, Mysyk R. Review on supercapacitors: Technologies and materials. Renewable and Sustainable Energy Reviews 2016;58:1189–206. https://doi.org/10.1016/j.rser.2015.12.249.

[2] Pal B, Yang S, Ramesh S, Thangadurai V, Jose R. Electrolyte selection for supercapacitive devices: a critical review. Nanoscale Adv 2019;1:3807–35. https://doi.org/10.1039/C9NA00374F.

[3] Zhao C, Liu Y, Beirne S, Razal J, Chen J. Recent Development of Fabricating Flexible Micro-Supercapacitors for Wearable Devices. Adv Mater Technol 2018;3. https://doi.org/10.1002/admt.201800028.

[4] Novoselov KS, Geim AK, Morozov S V., Jiang D, Zhang Y, Dubonos S V., et al. Electric Field Effect in Atomically Thin Carbon Films. Science (1979) 2004;306:666–9. https://doi.org/10.1126/science.1102896.

[5] Shams SS, Zhang R, Zhu J. Graphene synthesis: a Review. Materials Science-Poland 2015;33:566–78. https://doi.org/10.1515/msp-2015-0079.

[6] Clerici F, Fontana M, Bianco S, Serrapede M, Perrucci F, Ferrero S, et al. In situ MoS 2 Decoration of Laser-Induced Graphene as Flexible Supercapacitor Electrodes. ACS Appl Mater Interfaces 2016;8:10459–65. https://doi.org/10.1021/acsami.6b00808.

[7] Wang F, Wang K, Zheng B, Dong X, Mei X, Lv J, et al. Laser-induced graphene: preparation, functionalization and applications. Materials Technology 2018;33:340–56. https://doi.org/10.1080/10667857.2018.1447265.

[8] Zhang W, Lei Y, Ming F, Jiang Q, Costa PMFJ, Alshareef HN. Lignin Laser Lithography: A Direct-Write Method for Fabricating 3D Graphene Electrodes for Microsupercapacitors. Adv Energy Mater 2018;8. https://doi.org/10.1002/aenm.201801840.

[9] Mahmood F, Zhang H, Lin J, Wan C. Laser-Induced Graphene Derived from Kraft Lignin for Flexible Supercapacitors. ACS Omega 2020;5:14611–8. https://doi.org/10.1021/acsomega.0c01293.

[10] Lin J, Peng Z, Liu Y, Ruiz-Zepeda F, Ye R, Samuel ELG, et al. Laser-induced porous graphene films from commercial polymers. Nat Commun 2014;5:5714. https://doi.org/10.1038/ncomms6714.

[11] Shao Y, Li J, Li Y, Wang H, Zhang Q, Kaner RB. Flexible quasi-solid-state planar micro-supercapacitor based on cellular graphene films. Mater Horiz 2017;4:1145–50. https://doi.org/10.1039/C7MH00441A.

[12] Wu Y, Holze R. Self-discharge in supercapacitors: Causes, effects and therapies: An overview. Electrochemical Energy Technology 2021;7:1–37. https://doi.org/https://doi.org/10.1515/eetech-2020-0100.

[13] Abdisattar A, Yeleuov M, Daulbayev C, Askaruly K, Tolynbekov A, Taurbekov A, et al. Recent advances and challenges of current collectors for supercapacitors. Electrochem Commun 2022;142:107373. https://doi.org/10.1016/j.elecom.2022.107373.

[14] Remesh S, Vasudevan M, Perumal V, Ovinis M, Karuppanan S, Edison TNJI, et al. Oil palm lignin-derived laser scribed graphene in neutral electrolyte for high-performance microsupercapacitor application. J Environ Chem Eng 2023;11:110600. https://doi.org/10.1016/j.jece.2023.110600.

[15] Jyothibasu JP, Wang R-H, Tien Y-C, Kuo C-C, Lee R-H. Lignin-Derived Quinone Redox Moieties for Bio-Based Supercapacitors. Polymers (Basel) 2022;14:3106. https://doi.org/10.3390/polym14153106.

[16] Zhang L, Yan L, Wang Z, Laskar DD, Swita MS, Cort JR, et al. Characterization of lignin derived from water-only and dilute acid flowthrough pretreatment of poplar wood at elevated temperatures. Biotechnol Biofuels 2015;8:203. https://doi.org/10.1186/s13068-015-0377-x.

[17] Sekeri SH, Ibrahim MNM, Umar K, Yaqoob AA, Azmi MN, Hussin MH, et al. Preparation and characterization of nanosized lignin from oil palm (Elaeis guineensis) biomass as a novel emulsifying agent. Int J Biol Macromol 2020;164:3114–24. https://doi.org/10.1016/j.ijbiomac.2020.08.181.

[18] Subramani IG, Perumal V, Gopinath SCB, Mohamed NM, Ovinis M, Sze LL. 1,1'-Carbonyldiimidazole-copper nanoflower enhanced collapsible laser scribed graphene engraved microgap capacitive aptasensor for the detection of milk allergen. Sci Rep 2021;11:20825. https://doi.org/10.1038/s41598-021-00057-4.

[19] Mahmood F, Zhang C, Xie Y, Stalla D, Lin J, Wan C. Transforming lignin into porous graphene via direct laser writing for solid-state supercapacitors. RSC Adv 2019;9:22713–20. https://doi.org/10.1039/C9RA04073K.

[20] Ye R, Chyan Y, Zhang J, Li Y, Han X, Kittrell C, et al. Laser-Induced Graphene Formation on Wood. Advanced Materials 2017;29. https://doi.org/10.1002/adma.201702211.

[21] Wang S, Yu Y, Luo S, Cheng X, Feng G, Zhang Y, et al. All-solid-state supercapacitors from natural lignin-based composite film by laser direct writing. Appl Phys Lett 2019;115. https://doi.org/10.1063/1.5118340.

[22] Lei Y, Alshareef AH, Zhao W, Inal S. Laser-Scribed Graphene Electrodes Derived from Lignin for Biochemical Sensing. ACS Appl Nano Mater 2020;3:1166–74. https://doi.org/10.1021/acsanm.9b01795.

[23] Sinha K, Meng L, Xu Q, Wang X. Laser induction of graphene onto lignin-upgraded flexible polymer matrix. Mater Lett 2021;286:129268. https://doi.org/10.1016/j.matlet.2020.129268.

[24] Yuan M, Luo F, Rao Y, Wang Y, Yu J, Li H, et al. Laser synthesis of superhydrophilic O/S co-doped porous graphene derived from sodium lignosulfonate for enhanced microsupercapacitors. J Power Sources 2021;513:230558. https://doi.org/10.1016/j.jpowsour.2021.230558.

[25] Arshad F, Munir A, Kashif QQ, Haq T ul, Iqbal J, Sher F, et al. Controlled development of higher-dimensional nanostructured copper oxide thin films as binder free electrocatalysts for oxygen evolution reaction. Int J Hydrogen Energy 2020;45:16583–90. https://doi.org/10.1016/j.ijhydene.2020.04.152.

[26] Khan MA, Nayan N, Shadiullah S, Ahmad MK, Soon CF. Surface Study of CuO Nanopetals by Advanced Nanocharacterization Techniques with Enhanced Optical and Catalytic Properties. Nanomaterials 2020;10:1298. https://doi.org/10.3390/nano10071298.

[27] Svintsitskiy DA, Stadnichenko AI, Demidov DV, Koscheev SV, Boronin AI. Investigation of oxygen states and reactivities on a nanostructured cupric oxide surface. Appl Surf Sci 2011;257:8542–9. https://doi.org/10.1016/j.apsusc.2011.05.012.

[28] Jiang P, Prendergast D, Borondics F, Porsgaard S, Giovanetti L, Pach E, et al. Experimental and theoretical investigation of the electronic structure of Cu2O and CuO thin films on Cu(110) using x-ray photoelectron and absorption spectroscopy. J Chem Phys 2013;138. https://doi.org/10.1063/1.4773583.

[29] Liu Y, Ma L, Zhang D, Han G, Chang Y. A simple route to prepare a Cu 2 O–CuO–GN nanohybrid for high-performance electrode materials. RSC Adv 2017;7:12027–32. https://doi.org/10.1039/C6RA26535A.

[30] Sulcius A, Griskonis E, Zmuidzinaviciene N. Copper Dissoliution in Concentrated Sulfuric Acid. World Journal of Chemical Education 2019;7:196–202. https://doi.org/10.12691/wjce-7-3-2.

[31] Zhou B, Liu W, Gong Y, Dong L, Deng Y. High-performance pseudocapacitors from kraft lignin modified active carbon. Electrochim Acta 2019;320:134640. https://doi.org/10.1016/j.electacta.2019.134640.

[32] Milczarek G, Nowicki M. Carbon nanotubes/kraft lignin composite: Characterization and charge storage properties. Mater Res Bull 2013;48:4032–8. https://doi.org/10.1016/j.materresbull.2013.06.022.

[33] Thareja S, Kumar A. High Electrochemical Performance of 2.5 V Aqueous Symmetric Supercapacitor Based on Nitrogen-Doped Reduced Graphene Oxide. Energy Technology 2020;8. https://doi.org/10.1002/ente.201901339.

[34] Wang W, Lu L, Xie Y, Mei X, Tang Y, Wu W, et al. Tailoring the surface morphology and nanoparticle distribution of laser-induced graphene/Co3O4 for high-performance flexible microsupercapacitors. Appl Surf Sci 2020;504:144487. https://doi.org/10.1016/j.apsusc.2019.144487.

[35] Cao L, Zhu S, Pan B, Dai X, Zhao W, Liu Y, et al. Stable and durable laser-induced graphene patterns embedded in polymer substrates. Carbon N Y 2020;163:85–94. https://doi.org/10.1016/j.carbon.2020.03.015.

[36] Wu Y, Zhang Y, Liu Y, Cui P, Chen S, Zhang Z, et al. Boosting the Electrochemical Performance of Graphene-Based On-Chip Micro-Supercapacitors by Regulating the Functional Groups. ACS Appl Mater Interfaces 2020;12:42933–41. https://doi.org/10.1021/acsami.0c11085.

[37] Peng Z, Ye R, Mann JA, Zakhidov D, Li Y, Smalley PR, et al. Flexible Boron-Doped Laser-Induced Graphene Microsupercapacitors. ACS Nano 2015;9:5868–75. https://doi.org/10.1021/acsnano.5b00436.

[38] Liu H, Xie Y, Liu J, Moon K, Lu L, Lin Z, et al. Laser-induced and KOH-activated 3D graphene: A flexible activated electrode fabricated via direct laser writing for in-plane micro-supercapacitors. Chemical Engineering Journal 2020;393:124672. https://doi.org/10.1016/j.cej.2020.124672.

[39] Han M, He M, Wang G, Luo S. Phosphoric acid involved laser induced microporous graphene via proton conducting polybenzimidazole for high-performance micro-supercapacitors. J Power Sources 2021;514:230579. https://doi.org/10.1016/j.jpowsour.2021.230579.

[40] Hamed A, Hessein A, Abd El-Moneim A. Towards high performance flexible planar supercapacitors: In-situ laser scribing doping and reduction of graphene oxide films. Appl Surf Sci 2021;551:149457. https://doi.org/10.1016/j.apsusc.2021.149457.